Macromolecules

pubs.acs.org/Macromolecules Article

Enhanced Concentration Fluctuations in Model Polyelectrolyte Coacervate Mixtures along a Salt Isopleth Phase Diagram

Yuanchi Ma, Samim Ali,† and Vivek M. Prabhu*

Cite This: *Macromolecules* 2021, 54, 11338−11350 Read Online

ACCESS | Metrics & More | Article Recommendations | Supporting Information

ABSTRACT: A temperature (T)-versus-polymer concentration (c_p) representation leads to nonoverlapping coexistence curves prepared from different initial polymer concentrations along a salt isopleth of aqueous mixtures of charge-stoichiometric, oppositely charged polydisperse polyelectrolytes. This effect was explained by an unequal salt concentration (c_s) between equilibrating phases that improves the relationship between the common c_s-c_p representation and $T-c_p$ along a salt isopleth in terms of a $T-c_s-c_p$ phase envelope. Further quantification of the cloud points and spinodal temperatures predicts regions of metastability and instability with critical points on a salt isopleth phase diagram. As the cloud point is approached, the correlation length for concentration fluctuations far exceeds the chain dimensions with evidence of a crossover from mean field to fluctuation regime. The effective critical exponents for the divergence in the osmotic compressibility, via scattered intensity to zero angle and correlation length, γ_{eff} and ν_{eff}, respectively, deviates from the 3D Ising model. These static light-scattering measurements illustrate that concentration fluctuations are enhanced by polyelectrolyte chain association near the lower critical solution temperature.

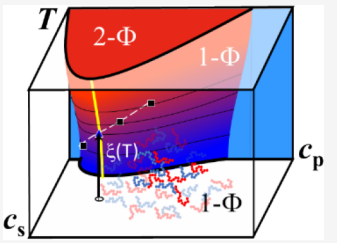

INTRODUCTION

The phase diagram of binary polymer blends and polymer solutions are commonly described by the Flory−Huggins (FH) mean-field theory with entropy of mixing from random mixing and the enthalpy of mixing from nearest-neighbor contacts modeled by the FH interaction parameter (χ).[1,2] This mean-field theory provides a conceptual framework to understand polymer mixtures and the effect of degree of polymerization (N).[3] Since the entropy of mixing scales as N^{-1}, small heats of mixing can lead to immiscibility. Near the critical point, an increase in concentration fluctuations leads to a crossover from mean-field behavior to a fluctuation regime that follows the 3D Ising model as quantified by the shape of the coexistence curve and divergence of the correlation length and susceptibility, with the reduced temperature, or distance from the critical temperature, defined by the Ginzburg criteria.[4] The interfacial tension of phase-separated polymer solutions also exhibits non-mean-field scaling with N and reduced temperature.[5] However, diluted critical mixtures observe deviations from Ising criticality and are explained by Fisher renormalization[6] with larger critical exponents for the divergence of the correlation length and susceptibility, ν and γ, respectively, as measured for binary polymer melts in the presence of a diluent,[7] critical polydisperse mixtures,[8] ternary solvents, and charged surfactant mixtures[9−11] as well as by computer simulation.[12]

When the polymers are charged, as in polyelectrolytes, the long-ranged electrostatic interactions must be considered with charge-neutralizing counterions in a medium of high dielectric constant, typically water, and added salt ions. The phase diagrams of polyelectrolyte solutions show a threshold phase separation on plots of salt concentration versus polymer concentration (c_s-c_p) and, in some, cases re-entrant and upper critical solution temperature (UCST) behavior.[13−15] A crossover from mean field to Ising behavior of aqueous semidilute sodium poly(styrene sulfonate) with $BaCl_2$ salt was observed by small-angle neutron scattering in a UCST system.[16]

Of present interest are the multicomponent aqueous mixtures or blends of oppositely charged polyelectrolytes. Such mixtures with or without salt exhibit properties with practical significance as adhesives,[17−19] structured membranes, and coatings[20] as well as vaccine adjuvants[21] and therapeutic delivery of proteins[22] and mRNA.[23] These mixtures undergo associative liquid−liquid phase separation into a polyelectrolyte-poor supernatant and polyelectrolyte-rich phase (coacervate) with an upper critical salt concentration[24,25] when studied as c_s-c_p phase diagrams at fixed temperature.[26−32] These multicomponent mixtures were first explained by the Voorn−Overbeek (VO) mean-field theory that extends the entropy of mixing from the FH theory to include the Debye−Hückel theory of electrolytes. The VO theory predicts phase separation under the simplifying assumptions of no account of intermolecular associations between oppositely charged polyelectrolytes, ion correlations are treated from dissolved

Received: September 22, 2021
Revised: November 23, 2021
Published: December 8, 2021

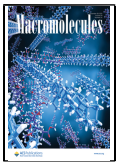

https://doi.org/10.1021/acs.macromol.1c02001
Macromolecules 2021, 54, 11338−11350

salt and decomposed polyelectrolyte, and no polymer−solvent enthalpic interactions (heat of mixing is zero).[33−35] Since the original VO theory, theoretical and computer simulation advances address many of these basic assumptions including evidence for the importance of counterion entropy[36−38] as recently reviewed.[24,39] In particular, when the ion correlations from the connectivity of the polyelectrolyte are included, the propensity of coacervation increases in terms of the critical charge density of the polyelectrolyte or critical salt concentration compared to the VO theory.[40] When the polymer−solvent interactions are included through χ, there is better agreement with binodal measurements.[26]

The van der Waals interaction energy, parameterized by χ, and the ion correlations are becoming increasingly important to explain recent measurements on coacervation. For example, c_s−c_p phase diagrams with homologous polyelectrolytes were fit by an extended VO theory that includes χ between the polyanion−polycation bound segment and solvent- and ion-binding equilibria for different Ns and polymer polarities.[30] A decrease in the critical salt concentration with lower charge density, controlled by hydrophilic ethylene oxide comonomer content, was observed with a different homologous polyelectrolyte system and compared to Gibbs ensemble computer simulations.[32] Lastly, mixtures of oppositely charged hydrophilic and hydrophobic polyelectrolytes, via aliphatic polymers or polypeptides, shift the c_s−c_p binodals and are explained by the solvent quality for the backbones via a combination of FH theory with an effective χ and ion correlations that include connectivity using the random phase approximation.[31]

Neutral polymer blends and oppositely charged polyelectrolyte mixtures straddle the more general problem of solvophobic phase separation and Coulombic phase separation, which on theoretical grounds expects classical exponents.[41] The scaling of the interfacial tension with reduced salt concentration were first observed by Spruit et al.[42] and Priftis et al.[43] They measure the interfacial tension scaling exponent (μ) in polyelectrolyte coacervates and expected by classical theory that $\mu = 3/2$.[44] Measurements closer to the critical salt concentration, also from within the two-phase region, did not observe deviations from the predicted classical scaling.[45,46] If the state of miscibility includes solvophobic contributions from χ, then oppositely charged polyelectrolyte mixtures should also exhibit phase separation driven by the temperature dependence of the polymer−solvent interactions. Recent measurements on potassium poly(styrene sulfonate) (KPSS) and poly(diallyldimethylammonium) bromide (PDADMAB) indeed show phase separation upon heating or lower critical solution temperature (LCST) behavior.[47] These results complement the known c_s−c_p phase diagrams[36,48] and expands the behavior to the T−c_p−c_s phase space. UCST was also observed under different conditions and interpreted as a solid−liquid phase transition, while the hydration state of the polyion binding plays a crucial role in the LCST.[49] Even though an LCST is not a natural result from the original FH theory with a single χ parameter, such behavior occurs theoretically by considering solvation,[50] hydrogen bonding,[51,52] and mutual and self-associations within the lattice cluster theory.[53] The temperature dependence of the static dielectric constant (ε) of the solvent appears in the strength of the ion correlations via the Bjerrum length (l_B) that equates thermal energy to the Coulombic potential energy between separated charges and the Debye screening length (κ^{-1}). Due to the temperature dependence of ε of water,[54,55] l_B slightly increases with increasing T and may contribute to the state of miscibility in addition to χ. The liquid state theory by Zhang et al. predicts an increase in l_B raises the c_s−c_p phase envelope, which is consistent with LCST behavior.[56] Adhikari et al. showed that the ion correlations and dipolar attractions of strength $\sim l_B^2$ strongly couples to the temperature dependence of χ leading to LCST, UCST, and mixed behavior depending on the choice of parameters.[57] These phase behaviors represent the complex interplay of solvophobic and electrostatic-driven phase separation in multicomponent mixtures (two polyelectrolytes, salt ions, and solvent) where the entropy of mixing of components, including contributions mediated by the counterion release upon ion binding, are all expected to play an active role in phase stability.[38] Such entropic origins of complexation due to small molecule counterion release,[58] enthalpic attraction,[59−61] and dipolar short-range interactions[38] provide unique characteristics when compared to neutral polymer blends and solutions. Additionally, since chain association or soluble complexes[62−64] form in the one-phase region, there is a need to understand how this couples to macrophase separation.[24]

A salt isopleth on the T−c_p plane allows for a convenient study of liquid−liquid phase separation and critical behavior starting from the one-phase region in mixtures of polyelectrolytes. This study addresses the pseudobinary coexistence curves, phase diagrams, and scattering properties in the one-phase region of the model system KPSS−PDADMAB complexes as charge-symmetric (1:1) mixtures upon approach to phase separation. The initial c_p and T were systematically varied with constant c_s (salt isopleth). Proton nuclear magnetic resonance (^{1}H NMR) and ultraviolet−visible (UV−Vis) spectroscopy measure an asymmetric distribution of the polycations and the polyanions in each phase to determine the points of total polymer concentration on the binodal, while static light scattering (SLS) and turbidity measurements were used to determine the spinodal and cloud point temperatures, respectively. The concentration fluctuations measured by SLS upon approach to the phase boundary were interpreted with the Ornstein−Zernike equation. We describe the mean field and crossover to fluctuation regime in the associative multicomponent mixtures of polyelectrolytes that complements neutral polymer solutions[65] and blends[66−68] and are consistent with Fisher renormalization near the critical point. The present studies propose concepts and phase diagram data to understand how the chain association of oppositely charged polyelectrolytes couples to fluctuations near the phase boundary that are projections along a three-dimensional T−c_s−c_p phase envelope with a line of critical points.

EXPERIMENTAL SECTION[A]

Materials. Sodium poly(styrene sulfonate) (NaPSS) and poly(diallyldimethylammonium chloride) (PDADMAC) were both purchased from Sigma-Aldrich. Characterization led to both polymers have charge fractions of 100%. The NaPSS and PDADMAC solutions were first ion-exchanged to give KPSS and PDADMAB, respectively. The procedures were as follows: 250 mL of 3 mol/L KBr solution was added to 20 mL of NaPSS (or PDADMAC) then pressed through an Ultracel ultrafiltration disc membrane (molecular mass cutoff = 3 kg/mol) by nitrogen pressure under mixing in an Amicon stirred cell equipped with a selector valve and a reservoir. This step was repeated four times so that the Na^+ (or Cl^-) was quantitatively replaced by K^+ (or Br^-). Diafiltration was then conducted to remove the excess KBr until the conductivity of the filtrate was negligible. The purified KPSS-and-PDADMAB solution were filtered through 0.22 μm cellulose

https://doi.org/10.1021/acs.macromol.1c02001
Macromolecules 2021, 54, 11338−11350

acetate membranes and then freeze-dried to yield dry polymer powder that was further heated to 120 °C under vacuum to remove residual water and then stored in a desiccator to avoid absorbing water from air. X-ray photoelectron spectroscopy (XPS) validated the quantitative exchange of Na^+ and Cl^- counterions to K^+ and Br^- (Figure S2). Aqueous size-exclusion chromatography led to substantially different molar mass characterization than from the manufacturer. Their relative mass-average molecular mass (M_w) and polydispersity ($Đ$) were characterized by size exclusion chromatography (SEC; Figure S1 of Supporting Information) with KPSS had an M_w = 196 kg/mol with $Đ$ = 2.8 and PDADMAB M_w = 60 kg/mol with $Đ$ = 2.76 relative to poly(2-vinyl pyridine) standards. These polymers were polydisperse and provide a working system to probe the phase behavior.

Preparation of Polyelectrolyte Complex Solutions. The purified, dry KPSS and PDADMAB were dissolved separately in ultrapure water to prepare 1.00 mol/L stock solutions. These stock solutions were added to predetermined volumes of aqueous KBr stock solution (4.00 mol/L) and vortex-mixed to give clear KPSS−KBr and PDADMAB−KBr solutions with known final salt concentration (c_s) and polymer concentration (c_p). The two solutions were then transferred to a separate 1.5 mL Eppendorf tube and mixed under vigorous agitation. The resulting polyelectrolyte complex solution was stored at 5 °C (below LCST) overnight prior to use.

Cloud Point Determination. The cloud point temperatures of the KPSS−PDADMAB complex solutions were determined by 532 nm wavelength laser light transmission, as defined by the inflection points of the transmission curves (Figure S3), upon heating at a rate of 0.2 °C/min.

Phase Separation and Extraction. The Eppendorf tube containing the polyelectrolyte complex solution was equilibrated in a water bath with temperature control with precision of ±0.1 °C (Isotemp, Fisher Scientific) for at least 2 h. When $T \geq 40$ °C, a DuraSeal film was placed between the tube and the lid to minimize the air gap, thus minimizing water evaporation during the equilibration. After the solution had phase-separated into two transparent phases with no visual droplets or cloudiness separated by a meniscus, the entire volume (700 to 2000 μL) of the supernatant was extracted by pipette into a separate vial. Following the prompt removal of the residual supernatant, 50 to 200 μL of the coacervate was extracted and diluted in 2.00 mol/L KBr solution in a separate vial.

UV−Visible Spectroscopy. The concentration of PSS was determined by UV−Vis spectroscopy with a PerkinElmer UV−Vis/NIR Lambda 900 Spectrometer. The supernatant and coacervate extracts were independently diluted to $c_p \approx (2 \times 10^{-4}$ to $1 \times 10^{-3})$ mol/L in a 1 cm path length quartz cuvette and measured for absorbance between 250 to 800 nm. PDADMAB has negligible UV−Vis absorbance over the entire wavelength range, while the PSS exhibits a known characteristic absorbance between 250 nm to 270 nm (Figure S4a). The PSS concentration (c_{PSS}) was determined using the absorbance at 262 nm and the Beer−Lambert law with a calibration curve valid up to $c_{PSS} = 1 \times 10^{-2}$ mol/L (Figure S4b).

^{1}H Nuclear Magnetic Resonance. ^{1}H NMR was conducted on a Bruker 600 UltraShield spectrometer with an autosampler. Prior to the experiments, the supernatant and the diluted coacervate extracts were dried under vacuum to completely remove water and then redissolved in predetermined amounts of D_2O containing 1.50 mol/L KBr and 5.51×10^{-3} mol/L 3-(trimethylsilyl) propionic-2,2,3,3-d_4 acid sodium salt (TMSP-d_4). The KBr in D_2O, together with the KBr in the dried extracts, added up to above 2 mol/L total salt concentration and therefore suppressed any phase separation in the ^{1}H NMR sample. The TMSP-d_4 served as the internal reference with which the integration area of the PSS^- and the $PDADMA^+$ peaks were compared so both concentrations can be determined. After this step, the samples were transferred into heavy-walled NMR tubes (Wilmad, 5 mm outer diameter, 2.2 mm inner diameter) and ^{1}H NMR spectra were collected. Even with the high salt concentration, the quality of the spectra was sufficient (Figure S5) to allow for integrations with an error of ≤10%. Because a proportion of protons were missing in the spectra regardless of the relaxation time T_1, resulting in the apparent decrease in the PSS^- and $PDADMA^+$ peak integration area relative to the theoretical values, a semiquantitative analysis was used. First, a series of ^{1}H NMR standards with known c_{PSS} and c_{PDADMA} were prepared so their S_A/S_R and S_C/S_R can be determined (S_A, S_C, and S_R stand for the peak integration area of the polyanion, polycation, and reference, respectively). As in the standards, the molar ratios between the polycations, the polyanions, and the reference are known; therefore, the theoretical peak integration area of the polyanions and the polycations, $S_{A,0}$ and $S_{C,0}$, can be calculated. The activity factors, α and β, are defined as $\alpha = S_A/S_{A,0}$ and $\beta = S_C/S_{C,0}$, which indicate the percentage of ^{1}H NMR-active protons in the two polyelectrolytes. They depend on c_s and c_p (Figure S6). It was observed that α and β are almost constant at $c_p \approx 0.050$ mol/L and c_s = (2.1 to 2.7) mol/L; therefore, all the dried samples were diluted to approximately this molarity, and α and β were applied to convert the ^{1}H NMR-active polymer concentrations to the actual concentrations in the samples.

Small-Angle Neutron Scattering. SANS measurements were conducted on the NGB30m beam line at National Institute of Standards and Technology (NIST) Center for Neutron Research, Gaithersburg, Maryland.[69] The configurations used an average neutron wavelength (λ) of 6.0 Å with wavelength spread ($\Delta\lambda/\lambda$) of 0.14. The scattering vector (q) range covered 0.003 to 0.5 $Å^{-1}$. Polyelectrolyte complex solutions in 1 mm quartz path-length banjo cells were thermostatically controlled within a nine-position temperature-controlled sample environment with ±0.1 °C precision. The temperature range of 16.2 to 19.8 °C were studied with an equilibration of 20 min prior to data collection. The two-dimensional scattering patterns collected by the image detector were reduced to absolute intensities and then azimuthally averaged and converted to 1D profiles as per standard protocols.[70]

Static Light Scattering. SLS measurements were performed with a modified Brookhaven BI-200SM using a wavelength of 532 nm laser light from a Coherent VERDI diode-pumped solid-state laser operating in TEM_{00} mode. The laser power was finely adjusted by neutral density filters. Glan-laser polarizer and analyzer (Thorlabs) were used under the vertical polarizer and vertical analyzer condition for all experiments. Samples contained within cylindrical glass cuvettes were placed in a decalin index-matching vat with temperature controlled by a recirculating bath to a precision of ±0.1 °C and sample temperature determined by a platinum resistance thermocouple placed within the vat. The scattered intensity (I_s) was collected between scattering angles of 20 to 140° in 10° increments enabled by the precision goniometer and detector arm. I_s was normalized by the angle-dependent scattering volume and reduced to Rayleigh ratio units under vv-polarization conditions (R_{vv}) using toluene scattering (I_{tol}) with the reference $R_{vv,tol} = 2.13 \times 10^{-5}$ cm^{-1} at 532 nm at 25 °C.[71] Dust-free samples were essential for SLS measurements, so all homogeneous, one-phase samples were filtered through 0.45 μm PVDF disc filters at 5 °C into clean, dust-free cylindrical light-scattering cells. For samples subject to higher temperature (>40 °C), a thick layer of silicone oil (5 cSt, Sigma-Aldrich) was added to the air/supernatant interface to suppress water evaporation.[72] The temperature was elevated toward the cloud points, determined by separate laser transmission experiments with 20 min equilibration time for each temperature increment. Independent measurements of the differential refractive index increment (dn/dc) reveal small differences between the polyelectrolyte in salt solutions, with values of 0.169 cm^3/g for KPSS and 0.155 cm^3/g for PDADMAB in 0.1 mol/L KBr at λ = 535 nm at 25 °C.

Estimating Critical Concentration. The sample preparation was conducted in a manner as described but within NMR tubes. Minimizing water evaporation was essential for reproducible results; therefore, as with SLS studies, a layer of silicone oil was used to minimize water evaporation. The NMR tube was immersed in a temperature-controlled water bath with precision of 0.1 °C and heated at 1 °C/h until the solution turned translucent. The sample was then held at this temperature to allow for phase separation into clear phases separated by a meniscus. Photographs were taken as soon as the meniscus was observed.

https://doi.org/10.1021/acs.macromol.1c02001
Macromolecules 2021, 54, 11338−11350

RESULTS AND DISCUSSION

Mixtures of oppositely charged polyelectrolytes may lead to liquid−liquid phase separation with an apparent upper critical salt concentration, LCST, and UCST. The following results examines in more depth the initial polymer concentration dependence and interrelationships of the common upper critical salt concentration with LCST behavior.

Polyelectrolyte Partitions Asymmetrically upon Liquid−Liquid Phase Separation. The effect of initial total polymer concentration ($c_{p,0}$) on the $T-c_p$ phase diagram was studied along a KBr salt isopleth. Figure 1a−c shows $c_{p,0}$s of 0.10, 0.20, and 0.30 mol/L, respectively, in moles of monomer repeat unit for KPSS and PDADMAB initially mixed at 1:1 stoichiometry by charge such that $c_{PSS,0} = c_{PDADMA,0} = (1/2)c_{p,0}$. The initial salt concentration ($c_{s,0}$), defined as the total concentration of the added salt and the polyelectrolyte counterions, was fixed at 1.80 mol/L. Under these conditions, the cloud point temperatures (T_{cp}) are near room temperature (Figure S3) and measured upon heating from $c_{p,0}$ and shown as solid green triangles.

Phase separation into polyelectrolyte-poor supernatant (left branch) and polyelectrolyte-rich dense coacervates (right branch) show an asymmetric polymer partitioning. UV−Vis measurements of the c_{PSS} illustrate the LCST behavior. However, the NMR measurements show that the supernatant has a concentration of PDADMA slightly higher than PSS, while in the coacervate, PSS is in excess. This information was absent in UV−Vis alone. While the partitioning of polymers appears unequal by charge, a conservation of mass from the initial concentration was verified such that $(c_{PSS,1}\cdot\phi_1 + c_{PSS,2}\cdot\phi_2)/c_{PSS,0} \approx (c_{PDADMA,1}\cdot\phi_1 + c_{PDADMA,2}\cdot\phi_2)/c_{PDADMA,0} = 1.0 \pm 0.1$ (Figure S7 and Table S1), with the subscripts 1 and 2 indicating the supernatant and the coacervate, respectively, and ϕ_i representing the volume fraction of each phase such that $\phi_1 + \phi_2 = 1$.

Figure 1 shows phase separation into nonstoichiometric polyion phases that differs from a common assumption of phase separation into equimolar associates. Nonstoichiometric polyelectrolyte complexes were observed in polyelectrolyte multilayers (PEMUs)[73−75] and solid polyelectrolyte complexes.[76,77] Porcel and Schlenoff analyzed the composition of a solid complex formed by 1:1 stoichiometry of NaPSS:PDADMAC and observed a molar ratio of 1.17:1 PSS:PDADMA after thorough rinsing with water to remove the supernatant and the excess counterions.[76] This is remarkably similar to our observations, considering the different sample preparation methods, molecular mass distribution of the polymers, counterions, and salt concentrations. They attributed the nonstoichiometric effect to the topological constraints in the polymer matrix that prevent complete complexation (intrinsic charge compensation) between polycations and polyanions, as well as the presence of mesoscale pores that may sequester free chains. A separate study observed that annealing the solid complex in 2.5 mol/L NaCl, the complex expelled extrinsic charges (counterions bound to the polyelectrolyte) from the pores and resulted in a 1:1 PSS:PDADMA composition.[78]

However, PEMUs and solid polyelectrolyte complexes are representative of kinetically frozen systems with high viscosity and low water content.[76,79,80] In contrast, the supernatant and coacervates in this study are highly hydrated and liquid-like, so the effect of topological constraints and porosity should not factor into the present study. This quantification of non-stoichiometry in the polyelectrolyte coacervates, starting from an initial 1:1 stoichiometry by charge, was unexpected. This behavior may be partially explained by preferential solvation of

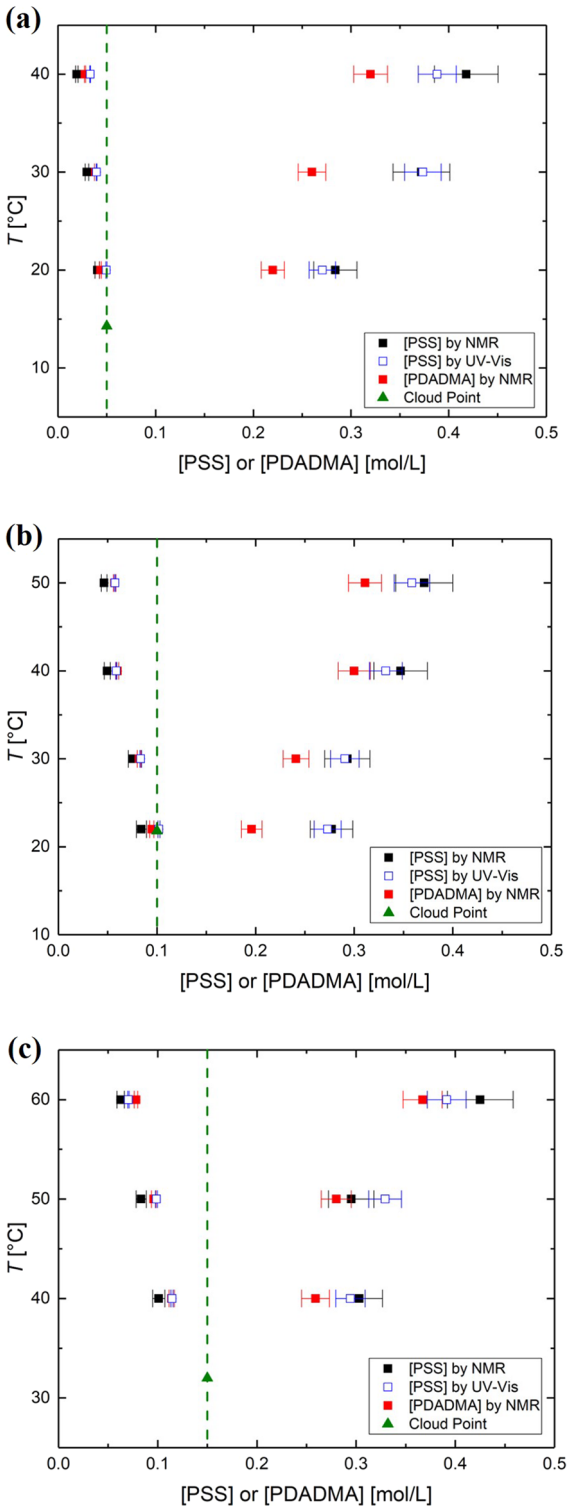

Figure 1. The pseudobinary coexistence curves of the phase-separated KPSS−PDADMAB complexes in H_2O with $c_{p,0}$s of (a) 0.10 mol/L, (b) 0.20 mol, and (c) 0.30 mol/L. The dashed vertical line marks the initial polymer concentration with the relationship of $c_{PSS} = c_{PDADMA} = c_{p,0}/2$. Error bars represent one standard deviation estimated from the uncertainty in the sampling micropipette volumes and NMR peak integrations averaged from five samples.

https://doi.org/10.1021/acs.macromol.1c02001
Macromolecules 2021, 54, 11338−11350

the polymers supported by the fact that KPSS precipitated in the presence of 4.0 mol/L KBr, while the PDADMAB did not (Figure S8). This solvent quality trend is consistent with the observations that NaPSS partially precipitated in 4.5 mol/L NaCl, while PDADMAC was soluble.[76] These solubility and solvation differences suggest a need for two different FH interaction parameters, χ,[31,81] whereas most analytical theories treat the polycations and polyanions as a pair represented by one effective interaction parameter (χ_{eff}) with the solvent. In the case of homologous polyelectrolytes that share the same backbone and differ only by the pendent charged group, a single χ_{eff} could quantify the c_s−c_p binodal measurements.[30] A modification of analytical theories with a separate χ between the polyanion and polycation with solvent may be sufficient to show unequal partitioning but also increases the complexity.[36,38] In such a case, under the same c_s and T, the effective interaction parameters of the polymer and solvent would be unequal such that $\chi_{PDADMA-water} < \chi_{PSS-water}$, which conceptually implies that PDADMA has preferential partitioning in the water-rich phase, leading to an excess of PSS in the coacervate. Such pair-wise interactions are directly incorporated into liquid-state theory with solvent as a continuum.[56]

While no phase diagrams were reported, UCST behavior[49] was observed in addition to LCST in the PSS/PDADMA complex with added KBr. The 1:1 stoichiometric mixtures by charge used a reported higher molecular mass of PSS than PDADMA, but no polydispersity or counterion exchange was reported. Such behavior was not observed by us across a wider range of polymer concentrations[49] and likely reflects additional complicating aspects of asymmetry of the chain length, polydispersity in molecular mass, and maintenance of one salt pair. The role of polydispersity cannot be ruled out, considering the dependence of molecular mass on binding.[82]

Pseudobinary Coexistence Curves in the T−c_p Plane. The three pseudobinary coexistence curves in Figure 1 are replotted in Figure 2 with the total polymer concentration $c_p = c_{PSS} + c_{PDADMA}$. Unexpectedly, these binodal curves do not overlap onto one curve. This shows that the pseudobinary representation is $c_{p,0}$-dependent near the cloud point on the T−c_p phase diagram.

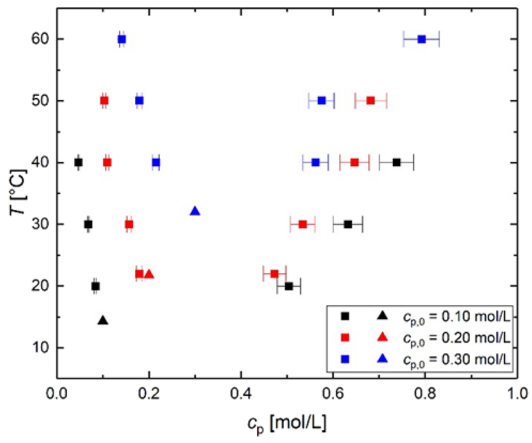

Figure 2. T−c_p phase diagram of KPSS−PDADMAB complexes in H_2O based on the NMR data from Figure 1. The square and triangle symbols represent the binodal points and the cloud points, respectively. Error bars represent one standard deviation estimated from the uncertainty in the sampling micropipette volumes and NMR peak integrations averaged from five samples.

Figure 2 shows a pronounced shift in the supernatant branches, more so than the coacervate branches. Additionally, under fixed c_s, higher $c_{p,0}$ is correlated with a lower propensity of phase separation, or smaller miscibility gap, as shown by the narrowing of the two-phase region. This new observation of an apparent $c_{p,0}$ dependence can be explained by considering negative tie lines in the c_s − c_p phase diagram (Figure 3a).[29,83,84]

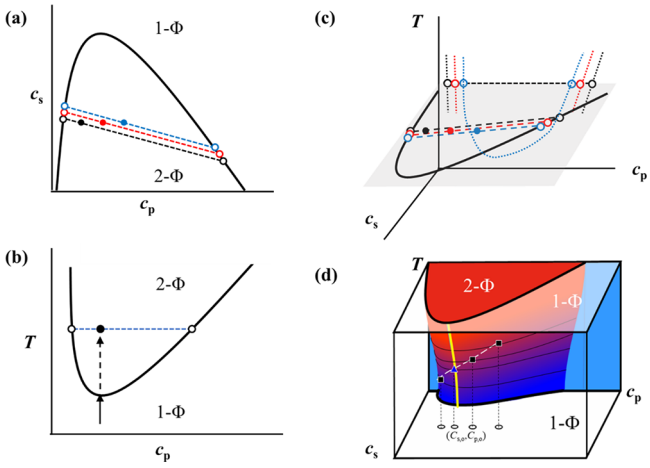

Figure 3. Schematics of two types of polyelectrolyte complex phase diagrams: (a) The c_s−c_p phase diagram showing negatively sloped tie lines (dashed lines) and resulting equilibrium phase concentrations (open symbols), starting from three different $c_{p,0}$s within the two-phase region (filled symbols). (b) The T−c_p phase diagram with dashed horizontal tie line connecting the supernatant and the coacervate branches (open symbols) from one $c_{p,0}$ (filled symbol). (c) T−c_s−c_p phase space in which the phase separation (solid symbols and dashed lines) takes place at fixed T and within the shaded c_s−c_p plane and projected upon the T−c_p plane. This leads to apparent $c_{p,0}$-dependent phase boundaries (open symbols and the dotted lines) along the c_p axis. (d) Envisioned 3D surface that shows how a line of critical points (yellow solid line) appears at the surface at different temperatures. Example initial concentrations are shown to meet the surface upon heating.

Figure 3a,c illustrates how to rationalize these pseudobinary observations. In Figure 3a, following the negatively sloped tie lines, any initial composition within the c_s−c_p phase envelope will phase separate into a polymer-rich, salt-poor phase and a polymer-poor, salt-rich phase. In this study, we fixed the initial salt concentration, $c_{s,0}$, and systematically increased $c_{p,0}$. This is equivalent to traversing horizontally through the c_s−c_p phase diagram parallel to the c_p axis. This is represented by the three colored solid symbols (black, red, and blue) in the order of increasing $c_{p,0}$. Assuming identical tie-line slopes,[29] these three $c_{p,0}$ will phase-separate into three pairs of different binodal points (open black, red, and blue circles), with the lowest $c_{p,0}$ having the largest polymer concentration difference in the two daughter phases. In Figure 3c, we consider the phase space with an additional vertical T axis of the same polyelectrolyte complex system. Under this scenario, the phase separation in the c_s−c_p plane is projected onto the T−c_p plane that align these binodal points along the isotherm with nonoverlapping features. For simplicity, Figure 3c only demonstrates the case of one temperature, but by inference, the $c_{p,0}$-dependence is a general feature for all Ts. Therefore, the connection of all binodals with identical $c_{s,0}$ will lead to multiple nonoverlapping

https://doi.org/10.1021/acs.macromol.1c02001
Macromolecules 2021, 54, 11338−11350

pseudobinary curves on the $T-c_p$ plane, one shown for example, which is consistent with our observations. This explanation provides a proof of concept in constructing a 3D phase diagram of polyelectrolyte complexes in Figure 3d that accounts for the pseudobinary observations. Figure 3d will be discussed in more depth in the sections on concentration fluctuations and the location of the critical polymer concentration along a salt isopleth. The overall miscibility gap would describe the LCST, such that at low temperature and high salt, only 1 Φ is present. Ylitalo et al.[85] independently predicted the nonoverlapping trends of the pseudobinary phase diagram (Figure 2) based upon a liquid-state theory for coacervation, which includes the essential physics, in particular, of the chain connectivity contributions to the electrostatic correlation term in the free energy and the temperature dependence of the solution dielectric constant. Their theory recovers a negative tie line on the c_s-c_p plane that is essential to predict the nonoverlapping pseudobinary diagrams with an LCST where higher polymer concentration led to an apparent narrowing and vertical shift. The opposite result would be observed with the Voorn−Overbeek theory because it predicts positive sloped tie lines, even though it may recover an LCST when considering the details of the dielectric constant. We expect alternate theoretical approaches to recover predictions similar to Figure 2 if plotted in the manner suggested.

Previous studies of two different $c_{p,0}$s ($c_{PSS,0}$ of 0.15 and 0.30 mol/L) at a higher fixed c_s = 2.0 mol/L KBr[47] show that increasing $c_{p,0}$ shifted the polymer-rich coacervate branch slightly to a higher concentration of PSS as measured by UV−Vis. The present study shows with more systematic data that higher $c_{p,0}$ leads to an upward shift of the binodal temperatures and narrowing of the miscibility gap. The differences between the two studies is most likely caused by a change in slope of the tie line on the c_s-c_p plane closer to the critical salt concentration at room temperature that can lead to a different projected (Figure 3c) shift on the pseudobinary representation. Secondary effects are improved purification methods and, especially, the counterion purity that was validated by XPS. The increase in the cloud point temperatures with increasing $c_{p,0}$ at fixed c_s remains the key conclusion by both studies but now with improved NMR methods to measure the concentrations.

Scattering Properties in the One-Phase Region Approaching the Cloud Point. The measurements of the pseudobinary phase diagrams are complemented by SANS and SLS within the one-phase region. SANS on the dense polyelectrolyte complexes have characterized the structure of the coacervate phase as well as chain conformation via a method of contrast variation or contrast-matching strategy.[78,86,87] The SANS study uses a full contrast approach where there are no deuterium-labeled chains; the contrast is provided by the hydrogen-rich polymers in salt-containing D_2O solvent, while SLS probes the refractive index fluctuations arising from solvent, polymer, and salt.

Figure 4 shows SANS and SLS data for c_s = 1.80 mol/L and $c_{p,0}$ = 0.30 mol/L with T_{cp} = 20.1 °C for a sample prepared in D_2O that illustrates the resolution limits. The SLS data are vertically scaled to the absolute-intensity SANS measurements by the scale factor b. Interestingly, SANS shows only a small increase in scattering at the lowest q (ranges indicated by arrows) as the sample is heated from 16.2 up to 0.3 °C below T_{cp}. The characteristic size (correlation length) cannot be reliably determined by SANS. However, the structure on the

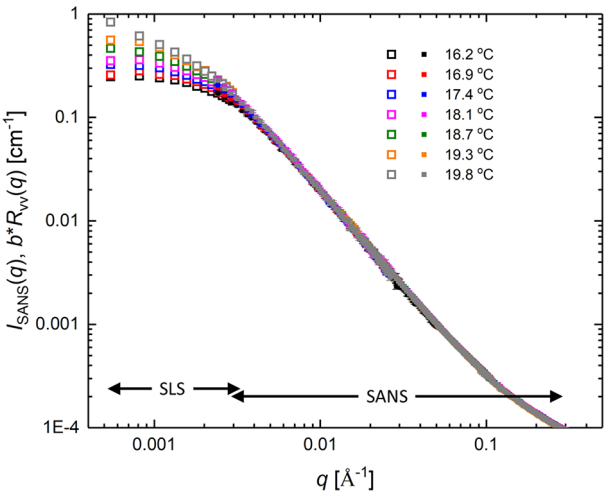

Figure 4. The full scattering profiles of KPSS−PDADMAB complex in D_2O (c_s = 1.80 mol/L; $c_{p,0}$ = 0.30 mol/L). The large and small symbols represent the data collected by SLS and SANS, respectively, from the same sample used for both measurements. To account for the contrast difference, all SLS data are vertically shifted by a factor of b = 0.00153 to match the SANS data.

chain dimension and segmental length scales are weakly dependent on temperature, and the mid-q region can be fit by a power law with $I(q)\sim q^{-D_F}$with fractal dimension (D_F) of 1.83 ± 0.05. The scattering spectrum is completed by SLS (low-q range) data. SLS provides a sensitive measurement of temperature-dependent concentration fluctuations at length scales defined by $1/q$. SLS was used to characterize these correlations within the one-phase region upon approaching T_{cp} in aqueous solutions.

The light-scattered intensities, $R_{vv}(q)$, systematically increase with T within the $c_{p,0}$ range from 0.10 to 0.60 mol/L. Figure 5

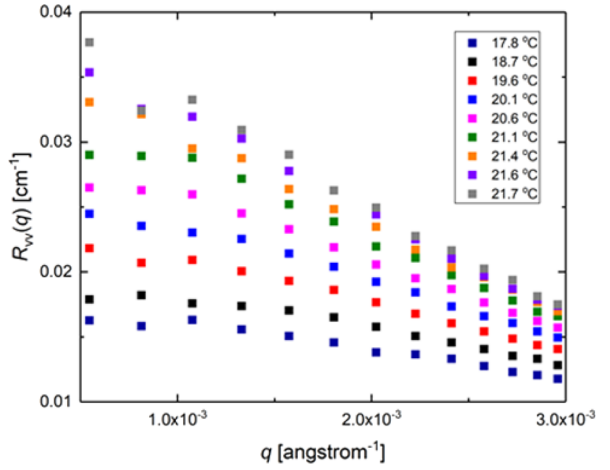

Figure 5. The SLS profiles of KPSS−PDADMAB complex in H_2O at various temperatures. This sample has $c_{p,0}$ of 0.20 mol/L, and its cloud point (T_{cp}) was determined to be 21.8 °C.

shows an example of the SLS profiles of $c_{p,0}$ = 0.20 mol/L from 17.8 to 21.7 °C. The intensity plateau at low-q ensures the largest scale fluctuations are measured as the two-phase region is approached. Additional $R_{vv}(q) - q$ plots (Figure S9) are in the Supporting Information.

Increase in Concentration Fluctuations near Phase Separation. The data, such as in Figure 5 and in the

https://doi.org/10.1021/acs.macromol.1c02001
Macromolecules 2021, 54, 11338−11350

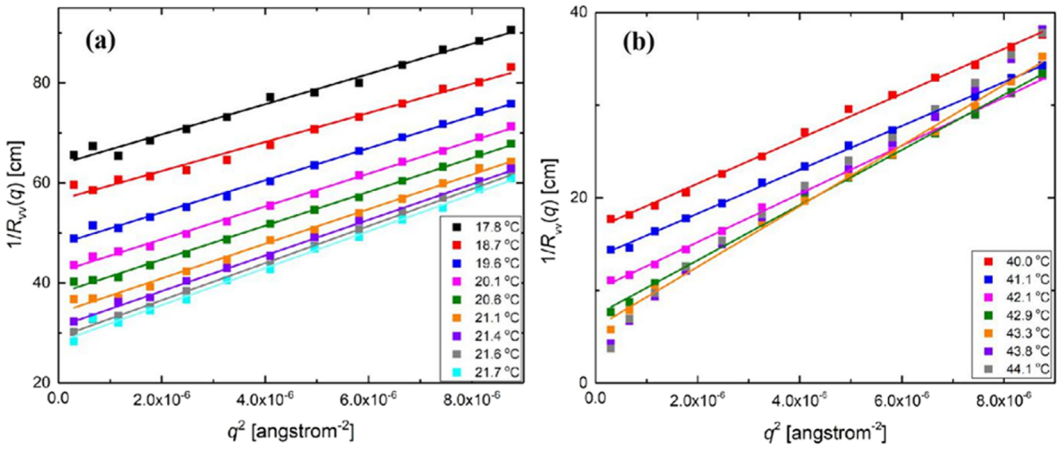

Figure 6. Representative Ornstein–Zernike plots $(R_{vv}(q)^{-1}$ vs $q^2)$ of KPSS–PDADMAB complexes at various temperature: (a) $c_{p,0}$ = 0.20 mol/L; (b) $c_{p,0}$ = 0.50 mol/L. The solid lines are best fit to the Ornstein–Zernike equation. In (b), nonlinearity arises above 43.3 °C.

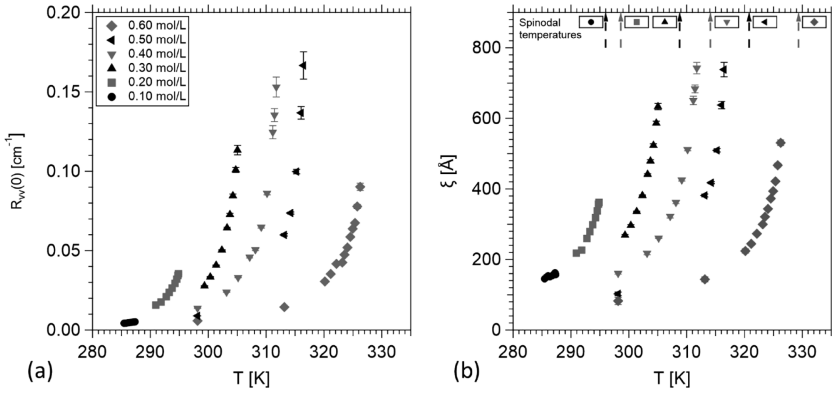

Figure 7. (a) The zero-angle scattered intensity, $R_{vv}(0)$, and (b) the correlation length, ξ, as a function of temperature. Arrows shows the extrapolated spinodal temperature corresponding to the concentration given by the symbols shown in (a). Uncertainties (error bars) are calculated as the estimated standard deviation from the linear regression fits to eq 1. While error bars are shown, they may be smaller than the symbols used.

Supporting Information, are quantified by the Ornstein–Zernike (OZ) equation with $R_{vv}(q)$ described by

$$R_{vv}(q) = R_{vv}(0)/(1 + q^2\xi^2) \quad (1)$$

where ξ is the correlation length of the concentration fluctuations and the zero-angle scattered intensity $R_{vv}(0)$. A typical OZ plot of Figure 6a shows fits to eq 1 over the entire q-range for each temperature between $c_{p,0}$ = 0.10 to 0.40 mol/L (Figure S10). Interestingly, at higher $c_{p,0}$, $R_{vv}(q)$ deviates from the OZ equation at the low-q and becomes time-dependent (Figures S10 and S11). The deviation and a time-dependent scattering occurs even after thermal equilibration, just below the cloud point temperature for $c_{p,0}$ = 0.50 mol/L (Figure 6b) and 0.60 mol/L (Figure S10d). Nonlinearity at low q in the OZ plots may arise from entering the metastable region where nucleation and growth takes place, leading to scattering by larger structures outside the instrument resolution or complications due to multiple scattering.[88−90] When this deviation occurred, as can be seen at 43.8 and 44.1 °C in Figure 6b, we take note of this temperature and exclude the data above this temperature from further OZ analysis and interpretation in order to present the most reliable estimates of ξ and $R_{vv}(0)$.

The temperature dependence of ξ and $R_{vv}(0)$ at different $c_{p,0}$ are shown in Figure 7. A divergence in ξ and $R_{vv}(0)$ as the temperature increases is observed at concentrations higher than 0.10 mol/L and is consistent with the approach to the LCST. The critical temperature (T_c) and spinodal temperatures (T_s) are estimated by extrapolation procedures from scattering data in binary polymer mixtures that can be quite complex with a crossover from mean field behavior to fluctuations.[91] Figure 7b shows the extrapolated T_s as the dashed vertical line for each concentration. We next explain how the spinodal points are estimated, followed by a discussion of the observations of fluctuations and how the critical polymer concentration was determined.

Characterization of the Spinodal Temperature. Near the critical and spinodal temperature, ξ and $R_{vv}(0)$ will diverge with characteristic scaling. The value of $R_{vv}(0)^{-1}$ is formally related to the susceptibility or isothermal osmotic compressibility by taking into consideration the prefactors for the scattering contrast.[92] In such a case, a free energy of mixing model for coacervation may be tested against systematic data, which is beyond the scope of the present study. We consider the main result that $R_{vv}(0)$ is a measure of the structure factor, such that $R_{vv}(0) \sim (\chi_s - \chi_{eff})^{-\gamma}$ where χ_s is the value of the Flory–Huggins interaction parameter at the spinodal line that may be predicted based upon a Gibbs free energy of mixing and χ_{eff} would have a characteristic temperature dependence. χ_{eff} may also include dependencies on the salt concentration via Debye screening length due to the screened electrostatic repulsion between charged segments as considered in

https://doi.org/10.1021/acs.macromol.1c02001
Macromolecules 2021, 54, 11338−11350

polyelectrolyte solutions[24] and between complexed polyelectrolyte segments and the solvent in coacervate phase diagrams.[26] The temperature and composition dependence of χ are often evaluated by SANS. The following are the expected dependencies for polymer mixtures if characterized by a single Flory–Huggins interaction parameter (χ) with an inverse temperature dependence and the spinodal $\chi_s \sim 1/T_s$

$$\xi \sim \left| \frac{1}{T_s} - \frac{1}{T} \right|^{-\nu} \tag{2}$$

$$R_{vv}(0) \sim \left| \frac{1}{T_s} - \frac{1}{T} \right|^{-\gamma} \tag{3}$$

In binary mixtures, mean-field theory predicts $\nu = 1/2$ and $\gamma = 1$, such that if ξ^{-2} and $R_{vv}(0)^{-1}$ are plotted versus $1/T$, a linear dependence would be expected far from the critical region as the phase transition is approached from the one-phase region. The exponents for binary mixtures with critical fluctuations are expected to follow Ising criticality with $\nu = 0.63$ and $\gamma = 1.26$.

Figure 8 displays $R_{vv}(0)^{-1}$ and ξ^{-2} versus inverse temperature for $c_{p,0} = 0.40$ mol/L. The linear dependence far from the phase boundary was expected by mean-field theory but with noticeable deviation. The linear dependence can define a mean-field spinodal temperature ($T_{s,mf}$), which are quite close between the two extrapolations that lead to an average of (310 ± 4) K. When considering the curvature, the estimate of T_s depends upon the method of extrapolation. We chose to simultaneously fit $R_{vv}(0)^{-1}$ and ξ^{-2} as a function of the reduced temperature ($\epsilon = |T - T_s| / T$) close to the phase boundary by excluding the linear region with eqs 4 and 5.

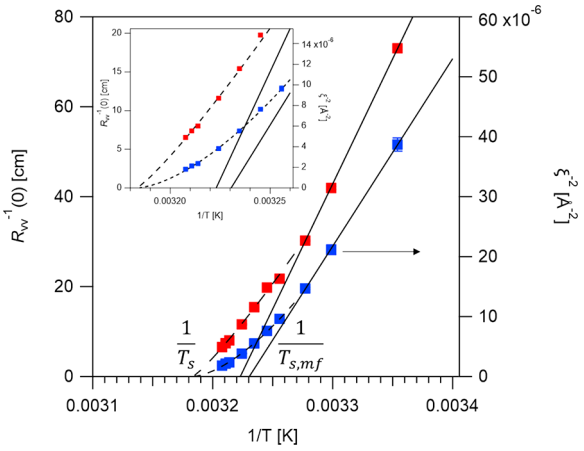

Figure 8. The $c_{p,0} = 0.40$ mol/L data for left axis, $R_{vv}(0)^{-1}$ (solid red squares), and right axis, ξ^{-2} (solid blue squares), as a function of $1/T$. The solid lines are independent fits that extrapolate to the mean-field spinodal temperature with fixed $\nu = 1/2$ and $\gamma = 1.0$, while the dashed lines are results from simultaneous fits to eqs 4 and 5 with a common T_s with nonlinear least squares regression with uncertainty weights. The inset provides an expanded view of the fits to the fluctuation model. The uncertainties (error bars) are estimated by one standard deviation to the fit and may be smaller than the symbols.

$$R_{vv}^{-1}(0) = R_{vv,0}^{-1} |\epsilon|^{\gamma_{eff}} \tag{4}$$

$$\xi^{-2} = \xi_o^{-2} |\epsilon|^{2\nu_{eff}} \tag{5}$$

By this method, a common T_s is estimated, which uses both datasets with two prefactor amplitudes ξ_o with dimension of length and $R_{vv,0}^{-1}$ with dimension of inverse scattered intensity, and two exponents ν_{eff} and γ_{eff} as fit parameters. A nonlinear regression with uncertainty weighting was used for a systematic study across the five highest concentrations with 0.40 mol/L shown in Figure 8. The lowest concentration (0.10 mol/L) did not show any curvature, and the mean-field expression was sufficient. The purpose of this analysis was to estimate T_s in a systematic way, while the effective indices and amplitudes provide added insight into the fluctuations and molecular scale details, respectively.

Salt Isopleth Phase Diagram with Critical Polymer Concentration. Figure 9 shows the cloud point (solid black squares) and spinodal (solid red circles) temperatures for all $c_{p,0}$s. When $c_{p,0} \leq 0.40$ mol/L, all T_ss are well above T_{cp}, such that the spinodal curve is within the cloud point phase envelope as expected. However, when $c_{p,0} \geq 0.50$ mol/L, an unexpected crossover between the cloud point and spinodal point occurs. In this concentration range, deviations from the OZ equation near T_{cp} were observed at low q. Even though the samples are in thermal equilibrium, there is a kinetic effect at these higher concentrations readily observable by SLS but not obvious by turbidity. We assume that the probability of nucleation remains low along with slow growth kinetics within the metastable region. The boundaries between the metastable and unstable regions are presently unknown in such polyelectrolyte complexes, but in light of this discrepancy, we add the temperature where the time-dependent scattering and deviation from OZ equation occurred to signify likely nucleation and growth with open black squares. The T_{cp} defined by the inflection point from a first derivative of the laser transmission curve cannot simply be slowed down from the programmed temperature heating rate (0.2 °C/min), since prolonged heating causes water evaporation. Evaporation and subsequent condensation near the sample cuvette cap increases the concentration and increases the T_{cp}. Evaporation was minimized by use of a mineral oil solvent trap.

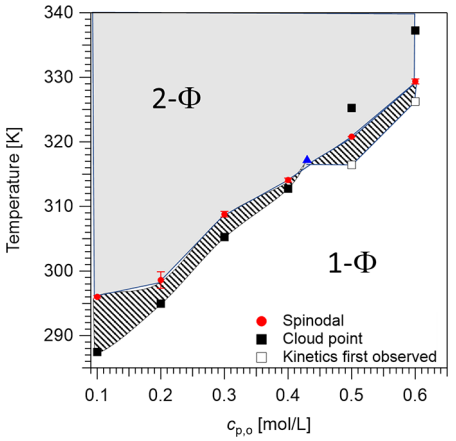

Figure 9. Salt isopleth phase diagram with T_{cp} and T_{sp} of KPSS–PDADMAB complexes with $c_{p,0} = 0.10$ to 0.60 mol/L at $c_s = 1.80$ mol/L of KBr. Predicted metastable region between the cloud point and spinodal point is shaded. Estimate critical polymer concentration and critical temperature are shown as solid blue triangles for near-symmetric tie lines. While error bars are shown, they may be smaller than the symbols used.

https://doi.org/10.1021/acs.macromol.1c02001
Macromolecules 2021, 54, 11338–11350

These results expand upon prior efforts[47] with higher polymer concentrations and, for the first time, the spinodal temperatures. Figure 9 represents a pseudobinary phase diagram formed by an initial salt isopleth. Each cloud point would represent one point on the $T-c_s-c_p$ phase surface upon heating as shown in Figure 3d from an initial polymer concentration. The region between the cloud point (or kinetic point) and the spinodal point suggests a narrow metastable region (hatched emphasis). Interestingly, a deep temperature quench should observe an unstable region with spinodal decomposition but passing through the metastable region, with exception to the critical point. Along these lines, notice that the cloud point and spinodal temperatures appear to converge from low polymer concentration and meet between $c_{p,0}$ = 0.4 to 0.5 mol/L in Figure 9. While this appears at an arbitrary polymer concentration, it can be rationalized to be a critical point by Figure 3d. In the $T-c_p$ phase diagram, the minima would meet at a critical point on the plot of c_s-c_p at fixed temperature. This will appear as a line of critical points (yellow line in Figure 3d) on the $T-c_s-c_p$ surface. The critical polymer concentration for a given salt isopleth will appear as a single point along a series of cloud points across multiple initial polymer concentrations of a salt isopleth as shown by the dashed line in Figure 3d and cloud points in Figure 9. Conceptually, the critical polymer concentration would occur at the point where the spinodal and binodal meet.

Measurements of the critical concentration and critical temperature is a challenging problem for complex fluids. Near the critical point, the properties exhibit universal features, but impurities, multiple components, and polydisperse polymers[93] introduce additional complications to compare with predictions. We sought to independently estimate the critical total polymer concentration ($c_{p,c}$) by examining the crossing of volume fractions via tie lines from different initial polymer concentrations. We estimate the KPSS–PDADMAB $c_{p,c}$ solution that phase-separates into equal volumes (tie lines equal) 50/50 (volume fraction) supernatant/coacervate as close to T_{cp} as possible.[65]

Figure 10 shows $c_{p,0}$ = 0.40 and 0.46 mol/L exhibited coacervate volume fractions of 0.40 and 0.62, respectively, which guided a concentration in between with a coacervate volume faction of 0.53 for $c_{p,0}$ = 0.43 mol/L closest to 50/50 (volume fraction) supernatant/coacervate, which is a signature of close to the critical condition in two-phase mixtures. From this concentration, the critical polymer volume fraction ($\phi_{p,c}$) at the critical temperature T_c = 44.0 °C and fixed salt concentration of 1.80 mol/L was estimated as $\phi_{p,c}$ = 0.059 using ρ_{KBr} = 2.75 g/cm^3 and ρ_{poly} = 1.13 g/cm^3, where ρ_{KBr} and ρ_{poly} are the mass densities of KBr and average of the polyelectrolytes. This critical temperature and $c_{p,c}$ are shown as solid blue triangles in Figure 9.

Apparent Critical Region and Crossover of Characteristic Length Scales Due to Chain Association. ξ increases from ~90 Å at $T < T_s$ to larger than 700 Å as $T \rightarrow T_s$ as shown in Figure 11 for $c_{p,0}$ = 0.40 mol/L. In order to put such results on an intuitive scale, consider that in dilute solution (0.02 mol/L) at the same 1.80 mol/L salt concentration, the hydrodynamic radius (R_h) of the KPSS and PDADMAB polymers are 75 and 63 Å, respectively (Figure S12). These R_h are an upper bound in chain dimensions, since polyelectrolyte size decreases with increasing polymer concentration from the dilute to semidilute regimes due to the screening of electrostatic and excluded volume interaction. In neutral

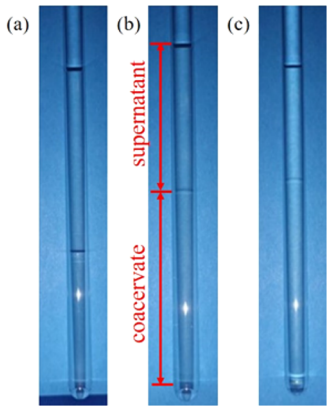

Figure 10. Photographs, slightly affected by the viewing angle or parallax, of the phase-separated KPSS–PDADMAB complexes with fixed 1.80 mol/L KBr, with $c_{p,0}$ = (a) 0.40 mol/L, (b) 0.43 mol/L, and (c) 0.46 mol/L. From bottom to top are coacervate, supernatant, and silicone oil. The phase separation temperatures for the samples in (a) to (c) are 42.1, 44.0, and 46.3°C; the resulting coacervate volume fractions are 0.40, 0.53, and 0.62, respectively, as measured from real samples.

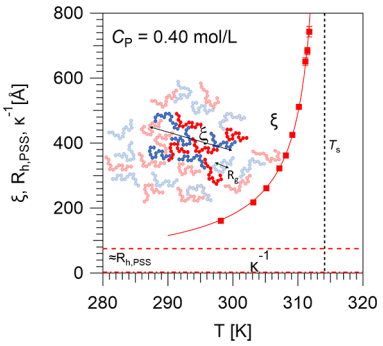

Figure 11. $\xi = (16.1 \pm 3.2)|\epsilon|^{-0.79 \pm 0.06}$[Å] with T_s being 314.1 ± 0.3 K. ξ far exceeds the characteristic length scales in polyelectrolyte solution, namely, the Bjerrum length (l_B = 7.1 Å at 25 °C) and Debye screening length (κ^{-1} = 2.3 Å at 25 °C and 1.8 mol/L 1:1 salt) even far from the phase boundary. The hydrodynamic radius of KPSS ($R_{h,PSS}$ = 75 Å) measured in dilute solution would be an upper limit in size. While error bars are shown, they may be smaller than the symbols used. Inset scheme shows the concepts of association and fluctuation length scale versus chain size.

polymer solutions, such as polystyrene in cyclohexane with well-defined phase diagrams, Melnichenko et al. showed by SANS that in the θ-region, $\xi < R_g$, while in the vicinity of the critical temperature, $\xi > R_g$.[94] The crossover length scale in the susceptibility (proportional to the scattered intensity) is the polymer size (R_g = 11 nm, in their case), such that Ising behavior occurs when $\xi > R_g$.[95] Interestingly, Schwahn and Pipich do not observe such a crossover criteria with aqueous solutions of associating poly(ethylene oxide).[96] The main result from the polyelectrolytes is that the dominant structural length scale becomes ξ and exceeds the expected chain dimensions even far from the phase boundary. The fluctuations and departure from mean-field behavior arises from the additional associative behavior of oppositely charged polyelectrolytes in the one-phase region, which is a distinguishing characteristic from neutral polymer solutions, such as polystyrene in cyclohexane. This associative behavior with D_f of 1.83 ± 0.05 must span multiple chains well below the phase

https://doi.org/10.1021/acs.macromol.1c02001
Macromolecules 2021, 54, 11338–11350

Table 1. Summary of Model Fit Parameters near the Spinodal Temperatures from Nonlinear Regression with Uncertainty Weights[a]

$c_{p,o}$ (mol/L)	ξ_o (Å)	ν_{eff}	$(R_{vv,0})^{-1}$ (cm)	γ_{eff}	T_s (K)
0.10	28.0 ± 0.3	0.5	0.189 ± 3 × 10^{-6}	1.0	296.0 ± 0.2
0.20	15.4 ± 9.7	0.72 ± 0.2	0.00026 ± 0.0002	1.1 ± 0.3	298.6 ± 1.3
0.30	12.0 ± 2.6	0.90 ± 0.07	0.00018 ± 6 × 10^{-5}	1.4_6 ± 0.1	308.8 ± 0.4
0.40	16.1 ± 3.2	0.79 ± 0.06	0.00054 ± 0.0002	1.16 ± 0.08	314.1 ± 0.3
0.50	6.4 ± 0.7	1.09 ± 0.03	0.00026 ± 3 × 10^{-6}	1.467 ± 0.004	320.80 ± 0.02
0.60	13.9 ± 0.4	0.78 ± 0.06	0.0011 ± 0.0002	0.94 ± 0.07	329.4 ± 0.4

[a]The error bars (uncertainties) in the fit parameters represent one standard deviation to the global fit to eqs 4 and 5 for each concentration.

boundary as shown by the relative values of ξ and $R_{h,PSS}$ in Figure 11. This result is different from LCST neutral polymers and gels that show D_f to vary from 5/3 to 2 with increasing temperature consistent with a change in solvent quality from good solvent to Θ conditions.[97] While these electrostatic-driven associations may appear through polycation−polyanion binding or dipolar attraction of ion pairs, the form was captured by the Landau−Ginzburg classical theory of fluctuations that gives rise to the observed OZ scattering. These fluctuations appear enhanced when far from conditions of macrophase separation through mesoscale soluble complexes (or inter-polyelectrolyte complexes) with sizes of >100 nm as observed in dilute solutions as studied for host−guest interactions,[64,98,99] simplexes,[63] stoichiometry of mixing,[62,100−102] and molecular mass.[82]

For $c_{p,0}$ = 0.40 mol/L, the reduced temperature varies between 0.0536 > ϵ > 0.0076 with effective indices ν_{eff} = 0.79 ± 0.06 and γ_{eff} = 1.16 ± 0.08, that deviate from mean-field theory and demonstrate the importance of fluctuations. The effective indices and amplitudes from simultaneous fits to eqs 4 and 5 are provided in Table 1. The critical amplitudes depend on the molecular details of the system[103] and show that ξ_o are smaller than the chain dimensions yet larger than expected by molecular liquids. Typically, $\gamma = 2\nu$, which was used for the lowest concentration; otherwise, we observe $\gamma_{eff} < 2\nu_{eff}$. This coincides with the theoretical relation of $\gamma = (2 - \eta)\nu$, where η is the correlation function exponent[104] that characterizes the shape of the structure factor at $q\xi > 1$, while binary mixtures may be characterized by one order parameter within a theory for fluctuations. The present water, salt, and two distinct polymers are multicomponent mixtures that complicate such interpretation with additional order parameters in concentration as well as those related to charge regulation.[24,105] Notably, diluted critical polymer blend mixtures are better described by Fisher's renormalized critical exponents, where γ' = 1.39 and ν' = 0.71.[7,8] Due to the high salt concentration and measurements near the critical concentration, these mixtures may represent highly diluted polymer blends when considering the observed exponents. However, this does not explain the broader phase diagram relationships and projection of pseudobinary mixtures. Further study of the critical exponents closer to the critical temperature at the critical concentrations may reveal if the current measurements have reached the asymptotic values.

CONCLUSIONS

The one-phase region in mixtures of oppositely charged polyelectrolytes exhibit concentration fluctuations that often appear as a low-q upturn in SANS measurements but are within SLS resolution. The one-phase region is not homogeneous due to the structure from the associative nature of polyelectrolytes mixtures that is enhanced near the LCST liquid−liquid phase-separation boundary. Within the phase envelope, an asymmetric partitioning of PSS and PDADMA was observed and speculated to be due to the difference in the solubility parameters for the separate polyelectrolytes in the presence of high KBr salt. In this respect, the enthalpic interactions, typically considered by a FH interaction parameter, may need interaction parameters between each polyion and solvent rather than one parameter. However, considering this complexity, when the phase diagrams are replotted in terms of temperature versus total polyelectrolyte concentration, the nonoverlapping coexistence curves are observed for different initial 1:1 stoichiometric mixtures of polymer concentrations. This logical result was due to the negative tie lines observed on the c_s−c_p phase diagrams and illustrate that the T−c_s−c_p phase diagrams would provide a miscibility gap surface with a line of critical salt and critical polymer concentrations at each temperature. Only one salt isopleth was studied in this respect and characterized by pseudobinary phase diagrams.

The spinodal temperatures within the T−c_p phase diagrams were characterized by Ornstein−Zernike scattering that follows the Landau−Ginzburg theory of fluctuations. The spinodal temperatures were estimated on a mean-field plot with effective critical indices and amplitudes. A crossover from mean-field to fluctuation regime was shown. This apparent critical behavior shows the correlation length far exceeds the expected chain dimensions and shift in the mean-field critical temperature. A crossover behavior was observed close to the measured critical polymer and salt concentration as discovered through equal volume observation. The effective critical indices with reduced temperature are not in quantitative agreement with the accepted 3D Ising values for binary mixtures but are consistent with deviations due to Fisher renormalization of diluted critical mixtures, such that the coacervate mixtures may theoretically behave as a highly diluted polymer blend. This may be a reasonable description if charged interactions are largely screened, yet these are multicomponent systems, not binary mixtures, so one does not expect 3D Ising criticality. The compelling evidence of large-scale fluctuations within the one-phase region, often observed as soluble complexes, show that chain association is enhanced near the phase boundary. A true test of Ising fluctuations would require attention to these phase diagrams with new proposed identification of the critical concentration.

ASSOCIATED CONTENT

Supporting Information

The Supporting Information is available free of charge at https://pubs.acs.org/doi/10.1021/acs.macromol.1c02001.

https://doi.org/10.1021/acs.macromol.1c02001
Macromolecules 2021, 54, 11338−11350

Additional $R_{vv}(q) - q$ and Ornstein−Zernike plots; X-ray photoelectron spectroscopy determination of counterion exchange; laser transmission curves to determine cloud point temperatures; example of UV−Vis spectra and calibration curve; SLS plots showing onset of kinetics of phase separation after thermal equilibration; polyelectrolyte hydrodynamic radius estimates; isotope effect on cloud point temperature (PDF)

AUTHOR INFORMATION

Corresponding Author

Vivek M. Prabhu − *Materials Science and Engineering Division, Material Measurement Laboratory, National Institute of Standards and Technology, Gaithersburg, Maryland 20899, United States;* orcid.org/0000-0001-8790-9521; Phone: (301)975-3657; Email: vprabhu@nist.gov

Authors

Yuanchi Ma − *Materials Science and Engineering Division, Material Measurement Laboratory, National Institute of Standards and Technology, Gaithersburg, Maryland 20899, United States*

Samim Ali − *Materials Science and Engineering Division, Material Measurement Laboratory, National Institute of Standards and Technology, Gaithersburg, Maryland 20899, United States*

Complete contact information is available at: https://pubs.acs.org/10.1021/acs.macromol.1c02001

Author Contributions

[†]Present address: Department of Chemical Engineering, Indian Institute of Technology Bombay, Powai, Maharashtra 400076, India.

Notes

The authors declare no competing financial interest.

ACKNOWLEDGMENTS

The authors are thankful for inspiring conversations with Jack Douglas (NIST), M. Muthukumar (University of Massachusetts-Amherst), and Zhen-Gang Wang and Andy Ylitalo (California Institute of Technology). The authors acknowledge partial support from the National Institute of Standards and Technology (NIST) Materials Genome Initiative and Dr. Yun Liu and Dr. Yimin Mao (NIST) for assistance with SANS measurements performed at the NIST Center for Neutron Research, Phillip Pickett (NIST) for SEC measurements, and Chris Stafford (NIST) for XPS measurements. Access to NGB30mSANS was provided by the Center for High Resolution Neutron Scattering (CHRNS), a partnership between the NIST and National Science Foundation under agreement no. DMR-1508249.

ADDITIONAL NOTE

[a]Certain equipment, instruments or materials are identified in this paper in order to adequately specify the experimental details. Such identification does not imply recommendation by the National Institute of Standards and Technology, nor does it imply the materials are necessarily the best available for the purpose.

REFERENCES

(1) Strobl, G. *The Physics of Polymers*; Springer-Verlag: Berlin, 1996.

(2) Rubinstein, M.; Colby, R. H. *Polymer Physics*; Oxford University Press, 2003.

(3) Gehlsen, M. D.; Rosedale, J. H.; Bates, F. S.; Wignall, G. D.; Hansen, L.; Almdal, K. Molecular Weight Scaling in Critical Polymer Mixtures. *Phys. Rev. Lett.* **1992**, *68*, 2452−2455.

(4) Anisimov, M. A.; Sengers, J. V. Scaling, Tricriticality, and Crossover in Polymer Solutions. *Mol. Phys.* **2005**, *103*, 3061−3070.

(5) Shinozaki, K.; van Tan, T.; Saito, Y.; Nose, T. Interfacial-Tension of Demixed Polymer-Solutions Near the Critical-Temperature - Polystyrene+methylcyclohexane. *Polymer* **1982**, *23*, 728−734.

(6) Fisher, M. E. Renormalization of Critical Exponents by Hidden Variables. *Phys. Rev.* **1968**, *176*, 257−272.

(7) Yajima, H.; Hair, D. W.; Nakatani, A. I.; Douglas, J. F.; Han, C. C. Dynamic Light-Scattering Study of a Diluted Polymer Blend near Its Critical Point. *Phys. Rev. B* **1993**, *47*, 12268−12271.

(8) Kita, R.; Kubota, K.; Dobashi, T. Static and Dynamic Light Scattering of a Critical Polydisperse Polymer Solution. *Phys. Rev. E* **1998**, *58*, 793−800.

(9) Chu, B.; Lin, F. L. Laser Light Scattering Study of a Ternary Liquid Mixture: Ethanol-water-chloroform. *J. Chem. Phys.* **1974**, *61*, 5132−5146.

(10) Ohbayashi, K.; Chu, B. Light Scattering near the Plait Point of a Ternary Liquid Mixture: Ethanol−Water−Chloroform. *J. Chem. Phys.* **1978**, *68*, 5066−5068.

(11) Kubota, K.; Kuwahara, N.; Sato, H. Critical Behavior of a Cationic Surfactant in an Aqueous Salt Solution. *J. Chem. Phys.* **1994**, *100*, 4543−4547.

(12) Dadmun, M. D.; Waldow, D. Effect of Added Copolymer on the Critical Properties of Polymer Mixtures. *Phys. Rev. E* **1999**, *60*, 4545−4550.

(13) de la Cruz, M. O.; Belloni, L.; Delsanti, M.; Dalbiez, J. P.; Spalla, O.; Drifford, M. Precipitation of Highly Charged Polyelectrolyte Solutions in the Presence of Multivalent Salts. *J. Chem. Phys.* **1995**, *103*, 5781−5791.

(14) Volk, N.; Vollmer, D.; Schmidt, M.; Oppermann, W.; Huber, K. Conformation and Phase Diagrams of Flexible Polyelectrolytes. In *Polyelectrolytes with Defined Molecular Architecture II*; Schmidt, M., Ed.; Advances in Polymer Science; Springer: Berlin, Heidelberg, 2004; pp. 29−65, DOI: 10.1007/b11348.

(15) Kanai, S.; Muthukumar, M. Phase Separation Kinetics of Polyelectrolyte Solutions. *J. Chem. Phys.* **2007**, *127*, 244908.

(16) Prabhu, V. M.; Muthukumar, M.; Wignall, G. D.; Melnichenko, Y. B. Polyelectrolyte Chain Dimensions and Concentration Fluctuations near Phase Boundaries. *J. Chem. Phys.* **2003**, *119*, 4085−4098.

(17) Lee, B. P.; Messersmith, P. B.; Israelachvili, J. N.; Waite, J. H. Mussel-Inspired Adhesives and Coatings. In *Annual Review of Materials Research, Vol 41*; Clarke, D. R.; Fratzl, P., Eds.; Annual Reviews: Palo Alto, 2011; Vol. *41*, pp. 99−132, DOI: 10.1146/annurev-matsci-062910-100429.

(18) Feldstein, M. M.; Dormidontova, E. E.; Khokhlov, A. R. Pressure Sensitive Adhesives Based on Interpolymer Complexes. *Prog. Polym. Sci.* **2015**, *42*, 79−153.

(19) Stewart, R. J.; Wang, C. S.; Song, I. T.; Jones, J. P. The Role of Coacervation and Phase Transitions in the Sandcastle Worm Adhesive System. *Adv. Colloid Interface Sci.* **2017**, *239*, 88−96.

(20) Sadman, K.; Delgado, D. E.; Won, Y.; Wang, Q.; Gray, K. A.; Shull, K. R. Versatile and High-Throughput Polyelectrolyte Complex Membranes via Phase Inversion. *ACS Appl. Mater. Interfaces* **2019**, *11*, 16018−16026.

(21) Andrianov, A. K.; Langer, R. Polyphosphazene Immunoadjuvants: Historical Perspective and Recent Advances. *J. Controlled Release* **2021**, *329*, 299−315.

(22) Black, K. A.; Priftis, D.; Perry, S. L.; Yip, J.; Byun, W. Y.; Tirrell, M. Protein Encapsulation via Polypeptide Complex Coacervation. *ACS Macro Lett.* **2014**, *3*, 1088−1091.
(23) McKinlay, C. J.; Vargas, J. R.; Blake, T. R.; Hardy, J. W.; Kanada, M.; Contag, C. H.; Wender, P. A.; Waymouth, R. M. Charge-Altering Releasable Transporters (CARTs) for the Delivery and Release of MRNA in Living Animals. *Proc. Natl. Acad. Sci. U. S. A.* **2017**, *114*, E448−E456.
(24) Muthukumar, M. 50th Anniversary Perspective: A Perspective on Polyelectrolyte Solutions. *Macromolecules* **2017**, *50*, 9528−9560.
(25) Sing, C. E.; Perry, S. L. Recent Progress in the Science of Complex Coacervation. *Soft Matter* **2020**, *16*, 2885−2914.
(26) Spruijt, E.; Westphal, A. H.; Borst, J. W.; Cohen Stuart, M. A.; van der Gucht, J. Binodal Compositions of Polyelectrolyte Complexes. *Macromolecules* **2010**, *43*, 6476−6484.
(27) Chollakup, R.; Smitthipong, W.; Eisenbach, C. D.; Tirrell, M. Phase Behavior and Coacervation of Aqueous Poly(Acrylic Acid)-Poly(Allylamine) Solutions. *Macromolecules* **2010**, *43*, 2518−2528.
(28) Priftis, D.; Tirrell, M. Phase Behaviour and Complex Coacervation of Aqueous Polypeptide Solutions. *Soft Matter* **2012**, *8*, 9396−9405.
(29) Li, L.; Srivastava, S.; Andreev, M.; Marciel, A. B.; de Pablo, J. J.; Tirrell, M. V. Phase Behavior and Salt Partitioning in Polyelectrolyte Complex Coacervates. *Macromolecules* **2018**, *51*, 2988−2995.
(30) Lou, J.; Friedowitz, S.; Qin, J.; Xia, Y. Tunable Coacervation of Well-Defined Homologous Polyanions and Polycations by Local Polarity. *ACS Cent. Sci.* **2019**, *5*, 549−557.
(31) Li, L.; Rumyantsev, A. M.; Srivastava, S.; Meng, S.; de Pablo, J. J.; Tirrell, M. V. Effect of Solvent Quality on the Phase Behavior of Polyelectrolyte Complexes. *Macromolecules* **2021**, *54*, 105−114.
(32) Neitzel, A. E.; Fang, Y. N.; Yu, B.; Rumyantsev, A. M.; de Pablo, J. J.; Tirrell, M. V. Polyelectrolyte Complex Coacervation across a Broad Range of Charge Densities. *Macromolecules* **2021**, *54*, 6878−6890.
(33) Voorn, M. J. Complex Coacervation .1. General Theoretical Considerations. *Recl. Trav. Chim. Pays-Bas* **1956**, *75*, 317−330.
(34) Voorn, M. J. Complex coacervation. II. Thermodynamic calculations on a specific model, with application to two component systems. *Recl. Trav. Chim. Pays-Bas* **1956**, *75*, 405−426.
(35) Michaeli, I.; Overbeek, J. T. G.; Voorn, M. J. Phase Separation of Polyelectrolyte Solutions. *J. Polym. Sci.* **1957**, *23*, 443−450.
(36) Salehi, A.; Larson, R. G. A Molecular Thermodynamic Model of Complexation in Mixtures of Oppositely Charged Polyelectrolytes with Explicit Account of Charge Association/Dissociation. *Macromolecules* **2016**, *49*, 9706−9719.
(37) Lytle, T. K.; Sing, C. E. Transfer Matrix Theory of Polymer Complex Coacervation. *Soft Matter* **2017**, *13*, 7001−7012.
(38) Adhikari, S.; Leaf, M. A.; Muthukumar, M. Polyelectrolyte Complex Coacervation by Electrostatic Dipolar Interactions. *J. Chem. Phys.* **2018**, *149*, 163308.
(39) Sing, C. E. Development of the Modern Theory of Polymeric Complex Coacervation. *Adv. Colloid Interface Sci.* **2017**, *239*, 2−16.
(40) Qin, J.; de Pablo, J. J. Criticality and Connectivity in Macromolecular Charge Complexation. *Macromolecules* **2016**, *49*, 8789−8800.
(41) Fisher, M. E. The story of coulombic critiality. *J. Stat. Phys.* **1994**, *75*, 1−36.
(42) Spruijt, E.; Sprakel, J.; Stuart, M. A. C.; van der Gucht, J. Interfacial Tension between a Complex Coacervate Phase and Its Coexisting Aqueous Phase. *Soft Matter* **2010**, *6*, 172−178.
(43) Priftis, D.; Farina, R.; Tirrell, M. Interfacial Energy of Polypeptide Complex Coacervates Measured via Capillary Adhesion. *Langmuir* **2012**, *28*, 8721−8729.
(44) Qin, J.; Priftis, D.; Farina, R.; Perry, S. L.; Leon, L.; Whitmer, J.; Hoffmann, K.; Tirrell, M.; de Pablo, J. J. Interfacial Tension of Polyelectrolyte Complex Coacervate Phases. *ACS Macro Lett.* **2014**, *3*, 565−568.
(45) Ali, S.; Prabhu, V. M. Characterization of the Ultralow Interfacial Tension in Liquid-Liquid Phase Separated Polyelectrolyte Complex Coacervates by the Deformed Drop Retraction Method. *Macromolecules* **2019**, *52*, 7495−7502.
(46) Prabhu, V. M. Interfacial Tension in Polyelectrolyte Systems Exhibiting Associative Liquid-Liquid Phase Separation. *Curr. Opin. Colloid Interface Sci.* **2021**, *53*, 101422.
(47) Ali, S.; Bleuel, M.; Prabhu, V. M. Lower Critical Solution Temperature in Polyelectrolyte Complex Coacervates. *ACS Macro Lett.* **2019**, *8*, 289−293.
(48) Wang, Q.; Schlenoff, J. B. The Polyelectrolyte Complex/Coacervate Continuum. *Macromolecules* **2014**, *47*, 3108−3116.
(49) Ye, Z.; Sun, S.; Wu, P. Distinct Cation-Anion Interactions in the UCST and LCST Behavior of Polyelectrolyte Complex Aqueous Solutions. *ACS Macro Lett.* **2020**, *9*, 974−979.
(50) Matsuyama, A.; Tanaka, F. Theory of Solvation-Induced Reentrant Phase Separation in Polymer Solutions. *Phys. Rev. Lett.* **1990**, *65*, 341−344.
(51) Andersen, G. R.; Wheeler, J. C. Theory of Lower Critical Solution Points in Aqueous Mixtures. *J. Chem. Phys.* **1978**, *69*, 3403−3413.
(52) Dormidontova, E. E. Role of Competitive PEO−Water and Water−Water Hydrogen Bonding in Aqueous Solution PEO Behavior. *Macromolecules* **2002**, *35*, 987−1001.
(53) Dudowicz, J.; Douglas, J. F.; Freed, K. F. Mixtures of Two Self- and Mutually-Associating Liquids: Phase Behavior, Second Virial Coefficients, and Entropy-Enthalpy Compensation in the Free Energy of Mixing. *J. Chem. Phys.* **2017**, *147*, No. 064909.
(54) Malmberg, C. G.; Maryott, A. A. Dielectric Constant of Water from 0 to 100 C. *J. Res. Natl. Bur. Stand.* **1956**, *56*, 1.
(55) Furia, T. E. *CRC Handbook of Chemistry and Physics*, 54th Edition.; Weast, R. C., Ed.; CRC Press, Inc., 1973.
(56) Zhang, P.; Alsaifi, N. M.; Wu, J.; Wang, Z.-G. Polyelectrolyte Complex Coacervation: Effects of Concentration Asymmetry. *J. Chem. Phys.* **2018**, *149*, 163303.
(57) Adhikari, S.; Prabhu, V. M.; Muthukumar, M. Lower Critical Solution Temperature Behavior in Polyelectrolyte Complex Coacervates. *Macromolecules* **2019**, *52*, 6998−7004.
(58) Priftis, D.; Laugel, N.; Tirrell, M. Thermodynamic Characterization of Polypeptide Complex Coacervation. *Langmuir* **2012**, *28*, 15947−15957.
(59) Ou, Z.; Muthukumar, M. Entropy and Enthalpy of Polyelectrolyte Complexation: Langevin Dynamics Simulations. *J. Chem. Phys.* **2006**, *124*, 154902.
(60) Fu, J.; Schlenoff, J. B. Driving Forces for Oppositely Charged Polyion Association in Aqueous Solutions: Enthalpic, Entropic, but Not Electrostatic. *J. Am. Chem. Soc.* **2016**, *138*, 980−990.
(61) Singh, A. N.; Yethiraj, A. Driving Force for the Complexation of Charged Polypeptides. *J. Phys. Chem. B* **2020**, *124*, 1285−1292.
(62) Pogodina, N. V.; Tsvetkov, N. V. Structure and Dynamics of the Polyelectrolyte Complex Formation. *Macromolecules* **1997**, *30*, 4897−4904.
(63) Philipp, B.; Dautzenberg, H.; Linow, K.-J.; Kötz, J.; Dawydoff, W. Polyelectrolyte Complexes — Recent Developments and Open Problems. *Prog. Polym. Sci.* **1989**, *14*, 91−172.
(64) Kabanov, V. A. Polyelectrolyte Complexes in Solution and in Bulk. *Russ. Chem. Rev.* **2005**, *74*, 3.
(65) Anisimov, M. A.; Kostko, A. F.; Sengers, J. V.; Yudin, I. K. Competition of Mesoscales and Crossover to Theta-Point Tricriticality in near-Critical Polymer Solutions. *J. Chem. Phys.* **2005**, *123*, 164901.
(66) Herkt-Maetzky, C.; Schelten, J. Critical Fluctuations in a Binary Polymer Mixture. *Phys. Rev. Lett.* **1983**, *51*, 896−899.
(67) Bates, F. S.; Rosedale, J. H.; Stepanek, P.; Lodge, T. P.; Wiltzius, P.; Fredrickson, G. H.; Hjelm, R. P., Jr. Static and Dynamic Crossover in a Critical Polymer Mixture. *Phys. Rev. Lett.* **1990**, *65*, 1893−1896.
(68) Schwahn, D.; Mortensen, K.; Yee-Madeira, H. Mean-Field and Ising Critical Behavior of a Polymer Blend. *Phys. Rev. Lett.* **1987**, *58*, 1544−1546.

https://doi.org/10.1021/acs.macromol.1c02001
Macromolecules 2021, 54, 11338−11350

(69) Glinka, C. J.; Barker, J. G.; Hammouda, B.; Krueger, S.; Moyer, J. J.; Orts, W. J. The 30 m Small-Angle Neutron Scattering Instruments at the National Institute of Standards and Technology. *J. Appl. Crystallogr.* **1998**, *31*, 430−445.
(70) Kline, S. R. Reduction and Analysis of SANS and USANS Data Using IGOR Pro. *J. Appl. Crystallogr.* **2006**, *39*, 895−900.
(71) Wu, H. Correlations between the Rayleigh Ratio and the Wavelength for Toluene and Benzene. *Chem. Phys.* **2010**, *367*, 44−47.
(72) Ali, S.; Prabhu, V. M. Relaxation Behavior by Time-Salt and Time-Temperature Superpositions of Polyelectrolyte Complexes from Coacervate to Precipitate. *GELS* **2018**, *4*, 11.
(73) Picart, C.; Lavalle, P.; Hubert, P.; Cuisinier, F. J. G.; Decher, G.; Schaaf, P.; Voegel, J. C. Buildup Mechanism for Poly(L-Lysine)/Hyaluronic Acid Films onto a Solid Surface. *Langmuir* **2001**, *17*, 7414−7424.
(74) Schlenoff, J. B.; Dubas, S. T. Mechanism of Polyelectrolyte Multilayer Growth: Charge Overcompensation and Distribution. *Macromolecules* **2001**, *34*, 592−598.
(75) Riegler, H.; Essler, F. Polyelectrolytes. 2. Intrinsic or Extrinsic Charge Compensation? Quantitative Charge Analysis of PAH/PSS Multilayers. *Langmuir* **2002**, *18*, 6694−6698.
(76) Porcel, C. H.; Schlenoff, J. B. Compact Polyelectrolyte Complexes: "Saloplastic" Candidates for Biomaterials. *Biomacromolecules* **2009**, *10*, 2968−2975.
(77) Hariri, H. H.; Schlenoff, J. B. Saloplastic Macroporous Polyelectrolyte Complexes: Cartilage Mimics. *Macromolecules* **2010**, *43*, 8656−8663.
(78) Markarian, M. Z.; Hariri, H. H.; Reisch, A.; Urban, V. S.; Schlenoff, J. B. A Small-Angle Neutron Scattering Study of the Equilibrium Conformation of Polyelectrolytes in Stoichiometric Saloplastic Polyelectrolyte Complexes. *Macromolecules* **2012**, *45*, 1016−1024.
(79) Dubas, S. T.; Schlenoff, J. B. Swelling and Smoothing of Polyelectrolyte Multilayers by Salt. *Langmuir* **2001**, *17*, 7725−7727.
(80) Jomaa, H. W.; Schlenoff, J. B. Salt-Induced Polyelectrolyte Interdiffusion in Multilayered Films: A Neutron Reflectivity Study. *Macromolecules* **2005**, *38*, 8473−8480.
(81) Kudlay, A.; Ermoshkin, A. V.; Olvera de la Cruz, M. Complexation of Oppositely Charged Polyelectrolytes: Effect of Ion Pair Formation. *Macromolecules* **2004**, *37*, 9231−9241.
(82) Karibyants, N.; Dautzenberg, H. Preferential Binding with Regard to Chain Length and Chemical Structure in the Reactions of Formation of Quasi-Soluble Polyelectrolyte Complexes. *Langmuir* **1998**, *14*, 4427−4434.
(83) Radhakrishna, M.; Basu, K.; Liu, Y.; Shamsi, R.; Perry, S. L.; Sing, C. E. Molecular Connectivity and Correlation Effects on Polymer Coacervation. *Macromolecules* **2017**, *50*, 3030−3037.
(84) Liu, Y.; Momani, B.; Winter, H. H.; Perry, S. L. Rheological Characterization of Liquid-to-Solid Transitions in Bulk Polyelectrolyte Complexes. *Soft Matter* **2017**, *13*, 7332−7340.
(85) Ylitalo, A. S.; Balzer, C.; Zhang, P.; Wang, Z.-G. Electrostatic Correlations and Temperature-Dependent Dielectric Constant Can Model LCST in Polyelectrolyte Complex Coacervation. *Macromolecules* **2021**, accepted, DOI: 10.1021/acs.macromol.1c02000.
(86) Spruijt, E.; Leermakers, F. A. M.; Fokkink, R.; Schweins, R.; van Well, A. A.; Cohen Stuart, M. A.; van der Gucht, J. Structure and Dynamics of Polyelectrolyte Complex Coacervates Studied by Scattering of Neutrons, X-Rays, and Light. *Macromolecules* **2013**, *46*, 4596−4605.
(87) Fares, H. M.; Ghoussoub, Y. E.; Delgado, J. D.; Fu, J.; Urban, V. S.; Schlenoff, J. B. Scattering Neutrons along the Polyelectrolyte Complex/Coacervate Continuum. *Macromolecules* **2018**, *51*, 4945−4955.
(88) Oxtoby, D. W.; Gelbart, W. M. Double-scattering-induced deviations from Ornstein-Zernike behavior near the critical point. *Phys. Rev. A* **1974**, *10*, 738−740.
(89) Hamano, K.; Kuwahara, N.; Kaneko, M. Scattered-Light Intensity in the Strongly Opalescent Region for the System Polystyrene-Diethyl Malonate. *Phys. Rev. A* **1980**, *21*, 1312−1315.
(90) Shanks, J. G.; Sengers, J. V. Double Scattering in Critically Opalescent Fluids. *Phys. Rev. A* **1988**, *38*, 885−896.
(91) Sengers, J. V.; Shanks, J. G. Experimental Critical-Exponent Values for Fluids. *J. Stat. Phys.* **2009**, *137*, 857−877.
(92) Horkay, F.; Burchard, W.; Geissler, E.; Hecht, A. M. Thermodynamic properties of poly(vinyl alcohol) and poly(vinyl alcohol-vinyl acetate) hydrogels. *Macromolecules* **1993**, *26*, 1296−1303.
(93) Kita, R.; Dobashi, T.; Yamamoto, T.; Nakata, M.; Kamide, K. Coexistence Curve of a Polydisperse Polymer Solution near the Critical Point. *Phys. Rev. E* **1997**, *55*, 3159−3163.
(94) Melnichenko, Y. B.; Wignall, G. D. Dimensions of Polymer Chains in Critical Semidilute Solutions. *Phys. Rev. Lett.* **1997**, *78*, 686−688.
(95) Melnichenko, Y. B.; Anisimov, M. A.; Povodyrev, A. A.; Wignall, G. D.; Sengers, J. V.; Van Hook, W. A. Sharp Crossover of the Susceptibility in Polymer Solutions near the Critical Demixing Point. *Phys. Rev. Lett.* **1997**, *79*, 5266−5269.
(96) Schwahn, D.; Pipich, V. Aqueous Solutions of Poly(Ethylene Oxide): Crossover from Ordinary to Tricritical Behavior. *Macromolecules* **2016**, *49*, 8228−8240.
(97) Shibayama, M.; Tanaka, T.; Han, C. C. Small angle neutron scattering study on poly (N-isopropyl acrylamide) gels near their volume-phase transition temperature. *J. Chem. Phys.* **1992**, *97*, 6829−6841.
(98) Kabanov, V. A.; Zezin, A. B. A New Class of Complex Water-Soluble Polyelectrolytes. *Makromol. Chem.* **1984**, *6*, 259−276.
(99) Izumrudov, V. A.; Bronich, T. K.; Zezin, A. B.; Kabanov, V. A. The Kinetics and Mechanism of Intermacromolecular Reactions in Poly-Electrolyte Solutions. *J. Polym. Sci., Polym. Lett. Ed.* **1985**, *23*, 439−444.
(100) Dautzenberg, H.; Hartmann, J.; Grunewald, S.; Brand, F. Stoichiometry and Structure of Polyelectrolyte Complex Particles in Diluted Solutions. *Berichte Bunsen-Ges.-Phys. Chem. Chem. Phys.* **1996**, *100*, 1024−1032.
(101) Karibyants, N.; Dautzenberg, H.; Cölfen, H. Characterization of PSS/PDADMAC-Co-AA Polyelectrolyte Complexes and Their Stoichiometry Using Analytical Ultracentrifugation. *Macromolecules* **1997**, *30*, 7803−7809.
(102) Webster, L.; Huglin, M. B.; Robb, I. D. Complex Formation between Polyelectrolytes in Dilute Aqueous Solution. *Polymer* **1997**, *38*, 1373−1380.
(103) Anisimov, M. A. *Critical Phenomena in Liquids and Liquid Crystals*; Gordon and Breach Science Publishers: Philadelphia, 1991.
(104) Janssen, S.; Schwahn, D.; Springer, T. Mean-field Ising crossover and the critical exponents γ, ν, and η for a polymer blend: d-PB/PS studied by small-angle neutron scattering. *Phys. Rev. Lett.* **1992**, *68*, 3180−3183.
(105) Lee, C.-L.; Muthukumar, M. Phase Behavior of Polyelectrolyte Solutions with Salt. *J. Chem. Phys.* **2009**, *130*, No. 024904.